GSA Data Repository 2020028

Craig, M.J., et al., 2020, Biomediation of submarine sediment gravity flow dynamics: Geology, v. 48, https://doi.org/10.1130/G46837.1

SUPPLEMENTARY INFORMATION

Methodology

Use of Xanthan Gum as an analogue for EPS

Xanthan gum, produced by the bacterium *Xanthomonas campestris*, was used as an analogue for EPS in these experiments because of its chemical and physical similarities with naturally occurring EPS (Steele et al., 2014). It has been common practice in a wide range of studies to substitute EPS for xanthan gum to simplify experiments and control conditions otherwise not possible when working with live bacteria (Rosenzweig et al., 2012).

Xanthan gum is not representative of all naturally occurring EPS. The diverse number of microorganisms that produce EPS, e.g. microalgae, phytoplankton, sea-ice diatoms, estuarine diatoms, bacteria and zooplankton, all secrete EPS with differ compositions for different functions i.e. adhesion, water retention, nutrient source, and enzyme activity (Krembs et al., 2011; Xiao and Zheng, 2016). The use of xanthan as a substitute for EPS in flume experiments is supported by the comparable rheological properties of aqueous solutions of natural EPS and xanthan because of their similarly high molecular weight (Fonseca et al., 2011; Morris et al., 2001; Xiao and Zheng, 2016). Some micro-algae produce polysaccharides that act as better drag-reducing additives than xanthan, rendering xanthan a possibly conservative choice of polymer to demonstrate the potential effects of EPS on sediment gravity flow dynamics (Gasljevic et al., 2008). Xanthan gum also enhances flocculation with increasing salinity in the same way as natural marine biopolymers; it is therefore suitable for use in a sediment-seawater mixtures representative of the marine environment (Furukawa et al., 2014). Beyond this, xanthan gum has been applied as an EPS analogue in studies of the protection of cells from hypersaline shock by EPS (Steele et al., 2014), EPS alteration of the formation of microstructures and salt retention in sea-ice (Krembs et al., 2011), and the effect of EPS on water retention in biofilm-affected soils (Rosenzweig et al., 2012).

Flume Experiments

In order to determine the effect of biological cohesion on physically-cohesive sediment gravity flows, 20 laboratory experiments were conducted in a 5.0 m long, 0.2 m wide and 0.5 m deep smooth-bottomed lock-exchange tank (Supplementary Figure 1). A 0.31 m long reservoir at the upstream end of the tank was filled with a mixture of kaolinite clay (D_{50} = 9.1 μm), EPS, and seawater to a depth of 0.35 m. The remainder of the tank contained seawater to the same depth. All seawater was sourced from the Menai Strait (North Wales, United Kingdom). Xanthan gum, a commercially available anionic hydrophilic biopolymer, was used as a proxy for natural EPS. The two compartments of the tank were separated by a lock gate, which was lifted to generate the gravity flow.

To account for any time-dependent behaviour of the mixture, each suspension was prepared using the same method. First, the xanthan gum and kaolinite clay were mixed dry in a concrete mixer for 10 minutes to evenly disperse the EPS within the clay. The seawater was then added to and mixed with the dry material for 10 min in the concrete mixer. Next, the wet mixture was decanted into a container and mixed again for 3 min using a handheld concrete mixer to break up any remaining clumps of sediment, before leaving it to rest for 60 min. At the end of the resting time, the suspension was mixed a third time for 3 min and then added to the reservoir of the lock-exchange tank. Here, it was mixed for a final 30 seconds; immediately thereafter the lock gate was lifted as quickly as possible to generate the sediment gravity flow.

A high-definition video camera tracked the head of the flow as it progressed along the tank. The velocity of the head of the flow was calculated using the time-stamped video frames and a reference scale along the bottom of the tank.

LabSFLOC-2 Methodology

Floc properties were measured using the LabSFLOC-2 (Laboratory Spectral Flocculation Characteristics) method. This method has been used successfully in numerous laboratory- and field-based flocculation studies and has demonstrated minimal floc disruption during acquisition (Manning et al., 2007; Mietta et al., 2009)[9]. LabSFLOC-2 uses a non-intrusive Puffin Paescon UTC 341 high-resolution video camera positioned 75 mm above the base of a square settling column (190x10x10 mm). This camera observes particles settling in the centre

of the column, using a depth of view of 1 mm at 45 mm in front of the lens. For the present experiments, the settling column was filled with seawater from the Menai Strait. To minimize density contrasts, care was taken to match the temperature with that of the seawater in the lock-exchange tank. A 0.4 m long glass pipette (4 mm internal diameter) was positioned in the lock-exchange tank at 60% of the anticipated flow run-out distance (based on an average of 12 replicate experiments). The end of the pipette was placed at 12 mm above the base of the tank, at the approximate height of the velocity maximum, informed by ultrasonic Doppler velocity profiler (UDVP) data. A small volume of mixed water, clay and EPS was then extracted from the passing head of the flow and immediately transferred to the LabSFLOC-2 settling column to minimise particle settling within the pipette. The sample was released from the pipette with the aperture of the pipette in contact with the water surface in the settling column through gravitational settling.

REFERENCES CITED

Fonseca, P. R., Dekker, R. F., Barbosa, A. M., Silveira, J. L., Vasconcelos, A. F., Monteiro, N. K., Aranda-Selverio, G., and Da Silva, M. d. L. C., 2011, Thermal and rheological properties of a family of botryosphaerans produced by Botryosphaeria rhodina MAMB-05: Molecules, v. 16, no. 9, p. 7488-7501.

Furukawa, Y., Reed, A. H., and Zhang, G., 2014, Effect of organic matter on estuarine flocculation: a laboratory study using montmorillonite, humic acid, xanthan gum, guar gum and natural estuarine flocs: Geochemical transactions, v. 15, no. 1, p. 1.

Gasljevic, K., Hall, K., Chapman, D., and Matthys, E., 2008, Drag-reducing polysaccharides from marine microalgae: species productivity and drag reduction effectiveness: Journal of applied phycology, v. 20, no. 3, p. 299-310.

Krembs, C., Eicken, H., and Deming, J. W., 2011, Exopolymer alteration of physical properties of sea ice and implications for ice habitability and biogeochemistry in a warmer Arctic: Proceedings of the National Academy of Sciences, v. 108, no. 9, p. 3653-3658.

Manning, A., Friend, P., Prowse, N., and Amos, C., 2007, Estuarine mud flocculation properties determined using an annular mini-flume and the LabSFLOC system: Continental Shelf Research, v. 27, no. 8, p. 1080-1095.

Mietta, F., Chassagne, C., Manning, A. J., and Winterwerp, J. C., 2009, Influence of shear rate, organic matter content, pH and salinity on mud flocculation: Ocean Dynamics, v. 59, no. 5, p. 751-763.

Morris, G., Li, P., Puaud, M., Liu, Z., Mitchell, J., and Harding, S., 2001, Hydrodynamic characterisation of the exopolysaccharide from the halophilic cyanobacterium Aphanothece halophytica GR02: A comparison with xanthan: Carbohydrate Polymers, v. 44, no. 3, p. 261-268.

Rosenzweig, R., Shavit, U., and Furman, A., 2012, Water retention curves of biofilm-affected soils using xanthan as an analogue: Soil Science Society of America Journal, v. 76, no. 1, p. 61-69.

Steele, D. J., Franklin, D. J., and Underwood, G. J., 2014, Protection of cells from salinity stress by extracellular polymeric substances in diatom biofilms: Biofouling, v. 30, no. 8, p. 987-998.

Xiao, R., and Zheng, Y., 2016, Overview of microalgal extracellular polymeric substances (EPS) and their applications: Biotechnology advances, v. 34, no. 7, p. 1225-1244.

SUPPLEMENTARY FIGURES

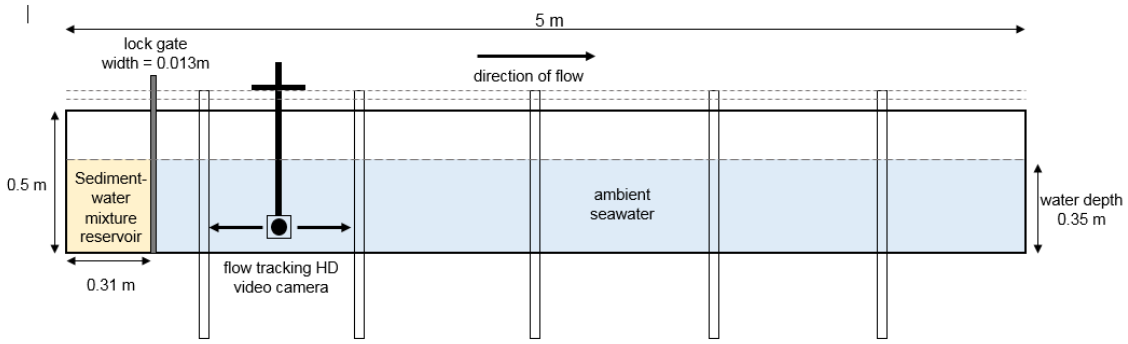

Supplementary Figure DR1 Schematic drawing of the lock-exchange tank.

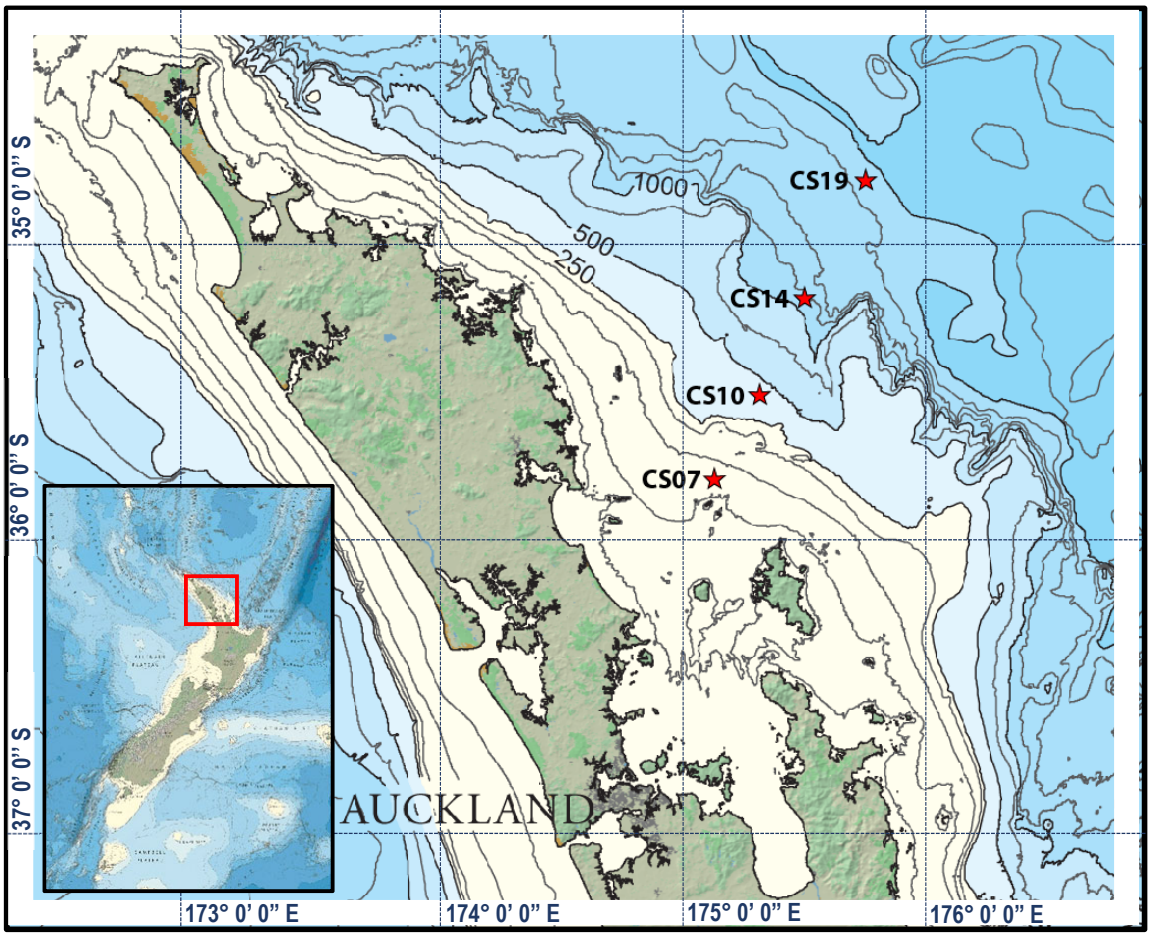

Supplementary Figure DR2 Outer Hauraki Gulf, New Zealand (see inset) with locations of core samples CS07 (127 m water depth), CS10 (432 m), CS14 (1149 m) and CS19 (1872 m) taken during RV Tangaroa cruise TAN1604. Samples were collected with an Ocean Instruments MC-800 multi-corer (10 cm diameter cores).

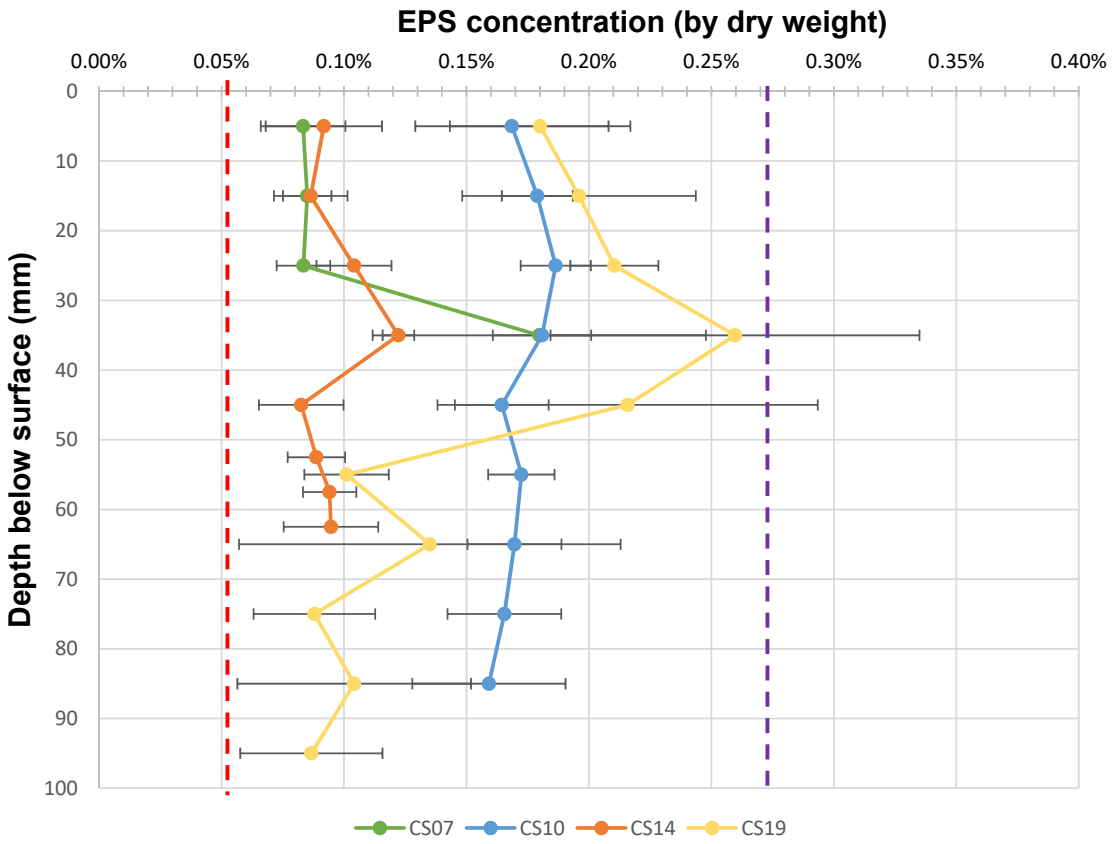

Supplementary Figure DR3 Vertical profiles of EPS taken from the outer Hauraki Gulf cores offshore New Zealand. The vertical lines represent dry weight quantities of EPS used within the experimental flows: (i) in red, 0.052% EPS in the bed reduced the run-out distance of a 23% kaolinite flow from 3.66 m (EPS-free equivalent) to 2.94 m; (ii) in purple, 0.259% EPS in the bed was the maximum amount of EPS used to simulate the 23% kaolinite flows, attaining a reduced run-out distance of 0.6 m. Horizontal lines denote standard deviation of the mean. Error bars correspond to the standard deviations (%) recorded for each EPS concentration (Supplementary Table DR1).

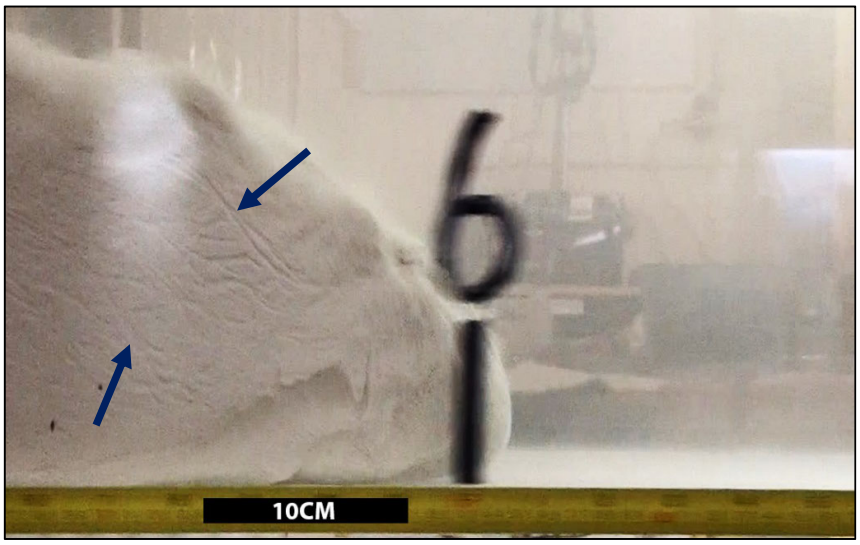

Supplementary Figure DR4: Head of F11, 22% clay TTPF without EPS at 1.8 m downstream of flow release. Run-out distance = 4.69 m. Note pronounced coherent fluid entrainment structures indicated by the dark blue arrows. Flow direction is from left to right.

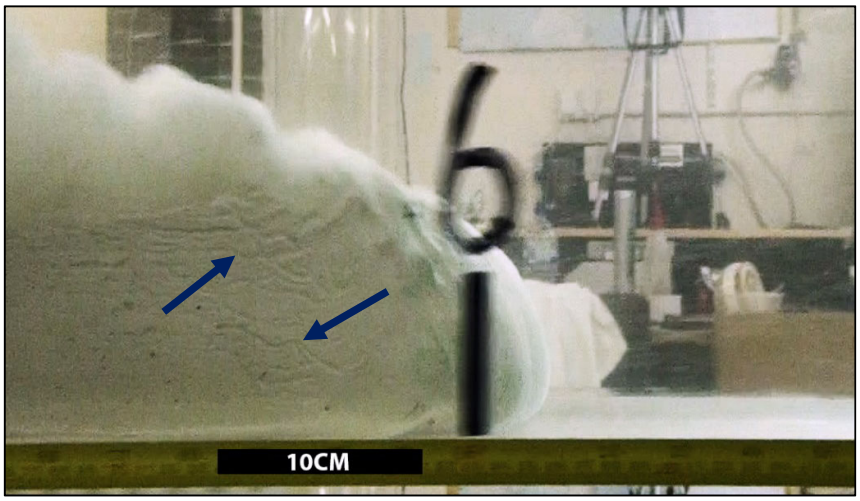

Supplementary Figure DR5: Head of F16, 23% clay TTPF without EPS at 1.8 m downstream of flow release. Run-out distance = 3.66 m. Note presence of coherent fluid entrainment structures indicated by the dark blue arrows. Flow direction is from left to right.

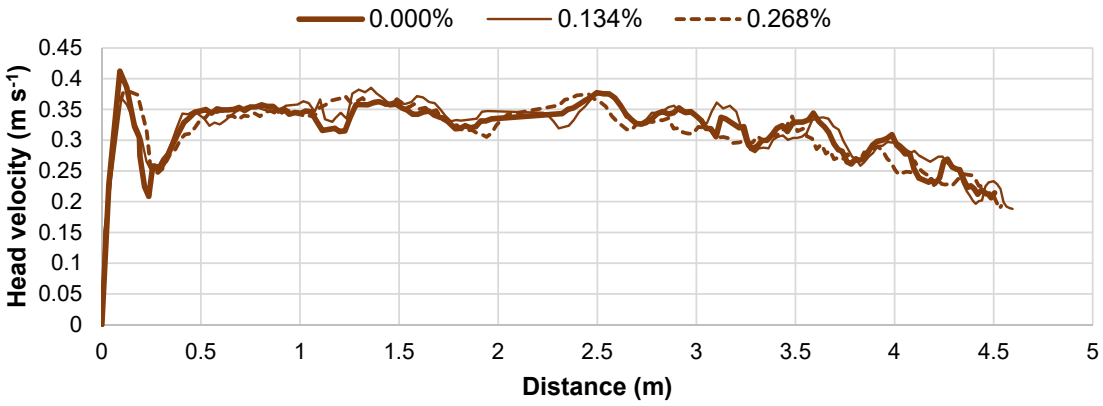

Supplementary Figure DR6: Head velocity of 5% kaolinite flows with and without EPS against distance travelled along the tank. Values in legend correspond to EPS concentration added.

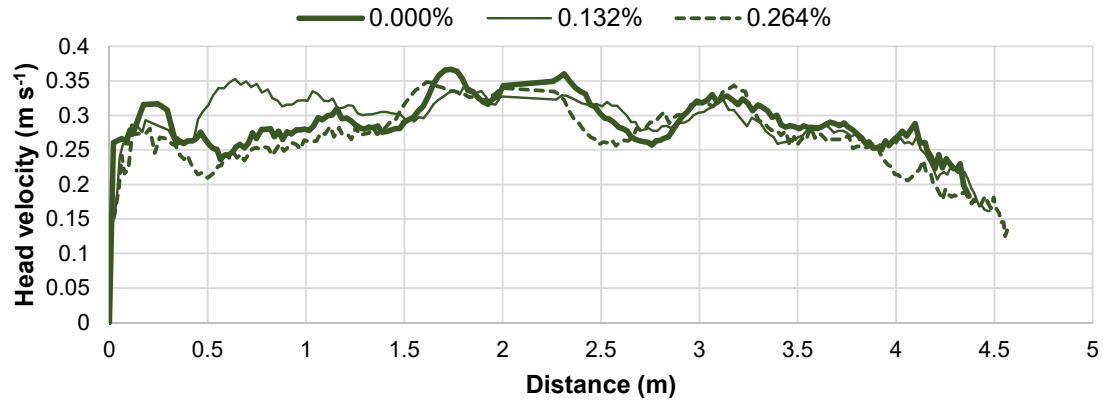

Supplementary Figure DR7: Head velocity of 10% kaolinite flows with and without EPS against distance travelled along the tank. Values in legend correspond to EPS concentration added.

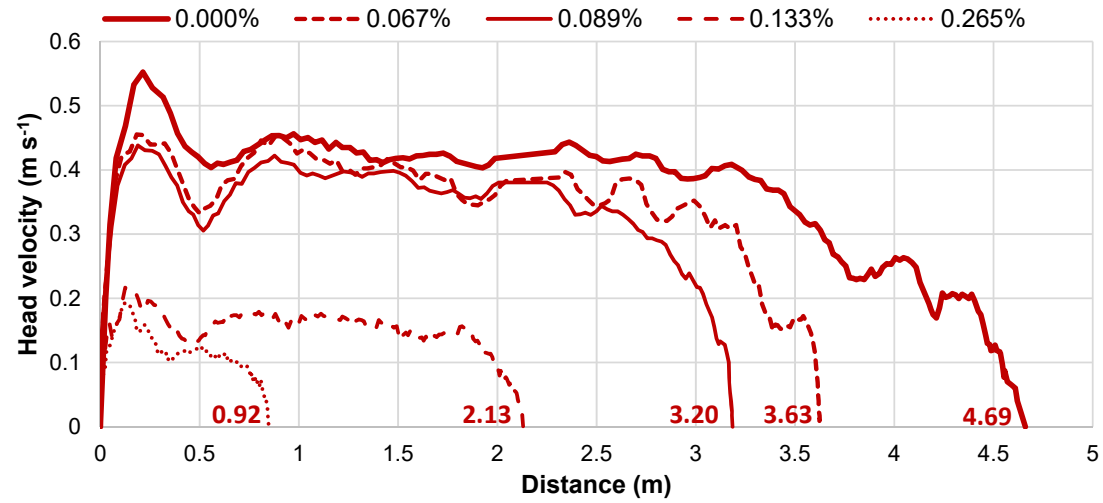

Supplementary Figure DR8: Head velocity of 22% kaolinite flows with and without EPS against distance travelled along the tank. Values in legend correspond to EPS concentration added. Numbers above the abscissa indicate run-out distances of flows.

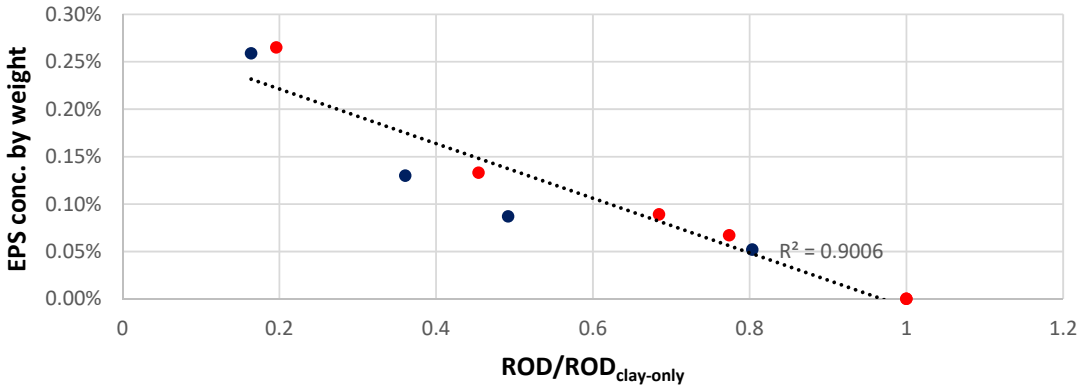

Supplementary Figure DR9: Normalized run-out distances of 22% (in red) and 23% (in blue) kaolinite flows with and without EPS against the EPS concentration by weight added to the flow. Run-out distances were normalized to their respective clay-only run-out distance. R^2 = 0.90, p<0.001, n=10.

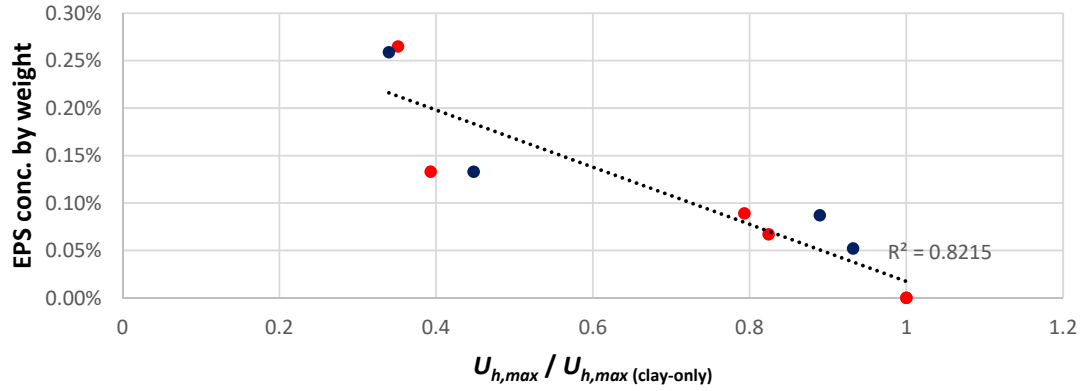

Supplementary Figure DR10: Normalized $U_{h,max}$ of 22% (in red) and 23% (in blue) kaolinite flows with and without EPS against the EPS concentration by weight added to the flow. $U_{h,max}$ values were normalized to their respective clay-only $U_{h,max}$ values. R^2 =0.82, p<0.001, n=10.

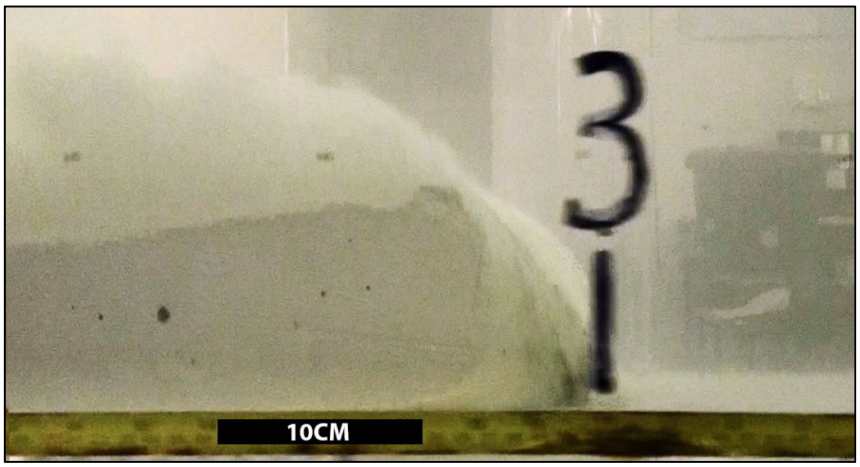

Supplementary Figure DR11: Head of F14, 22% clay plug flow with 0.133% EPS at 0.9 m downstream of flow release. Run-out distance = 2.13 m. Note absence of coherent fluid entrainment structures. Flow direction is from left to right.

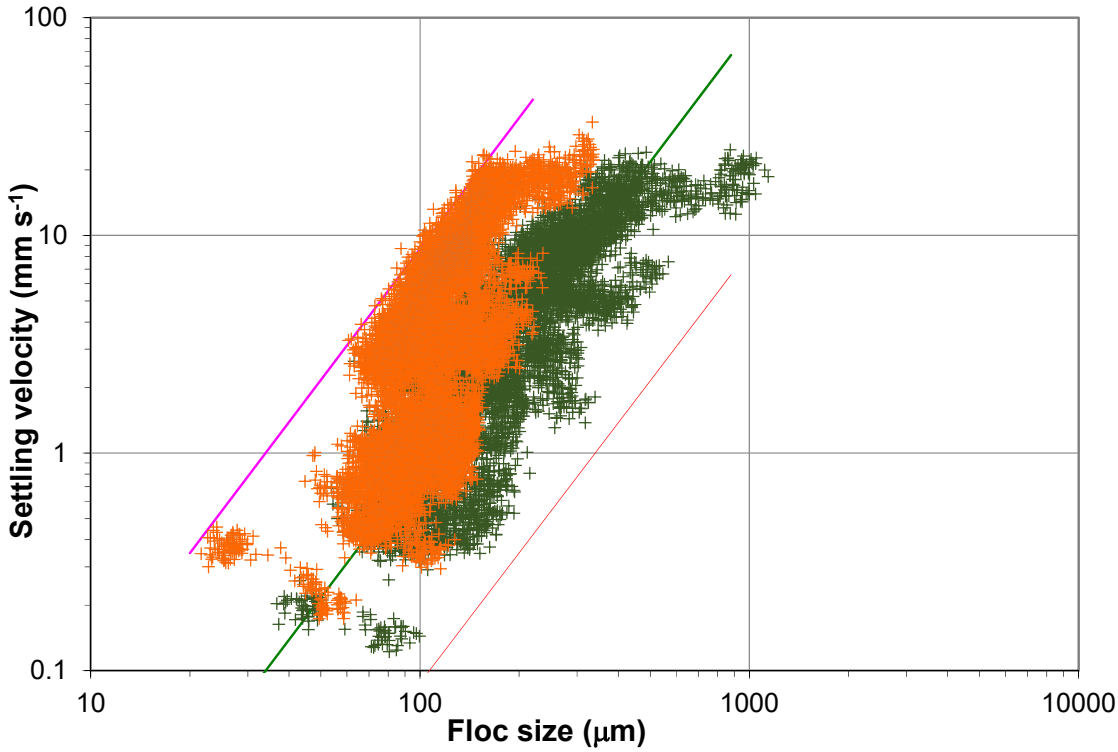

Supplementary Figure DR12 Distribution of floc size and settling velocity in samples extracted from the head of the EPS-free 23% kaolinite flow (in orange) and the 23% flow that carried 0.052% EPS (in green). Both samples were collected 12 mm above the base of the tank and at 60% of the respective run-out distance of each flow. Diagonal lines represent contours of constant Stokes-equivalent excess density: 1600 kg m^{-3} (in pink), 160 kg m^{-3} (in green) and 16 kg m^{-3} (in red).

Supplementary Table DR1 Summary of EPS data from cores collected during RV Tangaroa cruise TAN1604 in the outer Hauraki Gulf, New Zealand.

Core	*Depth (mm)*	*Total Carbohydrate, mean (%)*	*Total Carbohydrate, standard deviation (%)*	*D_{50} (µm)*	*Textural Description*
CS07	0-10	0.0833	0.0173	125.6	Slightly Gravelly Muddy Sand
CS07	10-20	0.0850	0.0099	97.42	Muddy Sand
CS07	20-30	0.0834	0.0109	69.52	Muddy Sand
CS07	30-40	0.1798	0.0680	49.23	Sandy Mud
CS10	0-10	0.1685	0.0395	74.75	Muddy Sand
CS10	10-20	0.1789	0.0145	88.49	Muddy Sand
CS10	20-30	0.1864	0.0143	93.73	Muddy Sand
CS10	30-40	0.1809	0.0201	93.73	Muddy Sand
CS10	40-50	0.1644	0.0192	93.73	Muddy Sand
CS10	50-60	0.1724	0.0136	81.16	Muddy Sand
CS10	60-70	0.1696	0.0192	81.61	Muddy Sand
CS10	70-80	0.1655	0.0232	82.68	Muddy Sand
CS10	80-90	0.1592	0.0313	77.13	Muddy Sand
CS14	0-10	0.0918	0.0237	64.69	Muddy Sand
CS14	10-20	0.0864	0.0150	63.01	Muddy Sand
CS14	20-30	0.1041	0.0153	81.13	Muddy Sand
CS14	30-40	0.1222	0.0065	81.13	Muddy Sand
CS14	40-50	0.0825	0.0173	81.13	Muddy Sand
CS14	50-55	0.0887	0.0117	83.05	Muddy Sand
CS14	55-60	0.0941	0.0109	83.05	Muddy Sand
CS14	60-65	0.0947	0.0193	71.57	Muddy Sand
CS19	0-10	0.1801	0.0368	15.00	Mud
CS19	10-20	0.1960	0.0477	15.44	Sandy Mud
CS19	20-30	0.2104	0.0180	14.88	Mud
CS19	30-40	0.2597	0.0753	14.42	Mud
CS19	40-50	0.2158	0.0777	14.33	Mud
CS19	50-60	0.1010	0.0172	15.53	Sandy Mud
CS19	60-70	0.1350	0.0779	20.16	Sandy Mud
CS19	70-80	0.0879	0.0248	18.47	Sandy Mud
CS19	80-90	0.1041	0.0477	17.16	Sandy Mud
CS19	90-100	0.0867	0.0290	16.28	Sandy Mud